Eur Biophys J (2011) 40:959–968
DOI 10.1007/s00249-011-0711-6

ORIGINAL PAPER

Folding dynamics of phenylalanine hydroxylase depends on the enzyme's metallation state: the native metal, iron, protects against aggregate intermediates

Aristobulo Loaiza · Judith A. Ronau · Alexander Ribbe · Lia Stanciu · John W. Burgner II · Lake N. Paul · Mahdi M. Abu-Omar

Received: 25 February 2011 / Revised: 7 April 2011 / Accepted: 28 April 2011 / Published online: 7 June 2011

Abstract Phenylalanine hydroxylase (PAH), a non-heme iron enzyme, is responsible for the phenylalanine conversion to tyrosine. Its malfunction causes phenylketonuria (PKU). To better understand how protein structure and folding profiles are affected by the metal cofactor, we investigated the chemical (un)folding of apo- and holo-PAH from *Chromobacterium violaceum* (cPAH) using circular dichroism (CD) and analytical ultracentrifugation (AUC). Holo-cPAH shows a two-state unfolding transition. In contrast, the unfolding profile for apo-cPAH reveals a three-state (un)folding pathway and accumulation of an intermediate (apo-cPAH^{I}). This intermediate is also observed in refolding experiments. Fluorescence studies are consistent with the CD findings. The intermediate apo-cPAH^{I} and unfolded state(s) of apo- and holo-cPAH^{U} have been characterized by analytical ultracentrifugation (AUC). At 2.4 and 2.8 M GuHCl, 90% of the signal for apo-cPAH has a weight average sedimentation coefficient in water at 20°C (s20,w) of about 48 S, representing multiple aggregate species made of multiple monomers of cPAH. Aggregate formation for apo-cPAH is also confirmed by dynamic light scattering and electron microscopy giving a hydrodynamic radius (R_H) of 41 nm for apo-cPAH^{I} versus 3.5 nm for the native protein.

Keywords Protein folding · Thermodynamics · Circular dichroism · Fluorescence · Metalloprotein · Analytical ultracentrifugation

Abbreviations

PAH	Phenylalanine hydroxylase
PKU	Phenylketonuria
cPAH	*Chromobacterium violaceum* phenylalanine hydroxylase
CD	Circular dichroism
AUC	Analytical ultracentrifugation
ANS	8-Anilino-1-naphthalene sulfonic acid
GuHCl	Guanidine hydrochloride
AAAHs	Aromatic amino acid hydroxylases
BH_4	Biopterin
DLS	Dynamic light scattering
TEM	Transmission electron microscopy
EPR	Electron paramagnetic spectroscopy

Electronic supplementary material The online version of this article (doi:10.1007/s00249-011-0711-6) contains supplementary material, which is available to authorized users.

A. Loaiza · J. A. Ronau · A. Ribbe · M. M. Abu-Omar (✉)
Brown Laboratory, Department of Chemistry, Purdue University, 560 Oval Drive, West Lafayette, IN 47907, USA
e-mail: mabuomar@purdue.edu

A. Loaiza
e-mail: aristobulo.loaiza@basf.com

J. A. Ronau
e-mail: jronau@purdue.edu

A. Ribbe
e-mail: ribbe@purdue.edu

L. Stanciu
School of Materials Engineering, Purdue University, Neil Armstrong Hall of Engineering, 701 West Stadium Avenue, West Lafayette, IN 47907, USA
e-mail: lstanciu@purdue.edu

J. W. Burgner II · L. N. Paul (✉)
Bindley Bioscience Center, Discovery Park, Purdue University, 1203 W. State Street, West Lafayette, IN 47907, USA
e-mail: lpaul@purdue.edu

J. W. Burgner II
e-mail: jburgner@purdue.edu

Introduction

Phenylalanine hydroxylase (PAH), a member of the aromatic amino acid hydroxylases (AAAHs) family, is a non-heme iron enzyme that catalyzes the hydroxylation of phenylalanine to tyrosine, which is the rate-determining step in the catabolism of phenylalanine (Fitzpatrick 2003; Kappock and Caradonna 1996). PAH's malfunction causes phenylketonuria (PKU). The enzyme requires iron(II), dioxygen (O_2), and biopterin cofactor (BH_4). Structural analysis of human PAH (hPAH) shows a mixed α/β tetrameric enzyme, comprised of three domains, an N-terminus regulatory domain, a C-terminus oligomerization domain, and a catalytic domain (Abu-Omar et al. 2005; Kobe et al. 1999).

Phenylalanine hydroxylase from *Chromobacterium violaceum* (cPAH) has been well studied due to both its relative structural simplicity and its structural similarity to the catalytic domain of human phenylalanine hydroxylase (hPAH). Whereas hPAH is comprised of three domains—regulatory, catalytic, and tetramerization—cPAH consists of a single domain (Abu-Omar et al. 2005; Kobe et al. 1999). Despite just 35% sequence homology between cPAH and hPAH, cPAH shares a near identical folding motif with the catalytic domain of hPAH (Fusetti et al. 1998) and can be superimposed with an RMSD of 1.2 Å (Fig. 1). The active site of both human and bacterial PAH contains iron(II) coordinated to six ligands (a His-His-Glu catalytic triad and water) in octahedral geometry with a slight difference: in cPAH, Glu 184 coordinates iron in a bidentate fashion and two water ligands, whereas hPAH features a monodentate Glu and three water ligands. Other differences have been observed between bacterial and human PAH. Erlandsen et al. (2002) stipulated that the active site in cPAH is more solvent-exposed than hPAH, likely making it more prime for hydroxylation of phenylalanine.

Even though earlier reports in the literature had described cPAH as copper-dependent (Pember et al. 1986) and subsequently metal-independent (Carr et al. 1995), our research group and others have shown unequivocally that cPAH is an iron enzyme (Chen and Frey 1998; Panay and Fitzpatrick 2008; Volner et al. 2003), and its activity is inhibited by other divalent metals such as Zn^{2+}, Cu^{2+}, and Co^{2+} (Zoidakis et al. 2005).

Most studies of wild-type and mutant forms of eukaryotic PAH have sought to unravel the structural basis of PKU (Erlandsen and Stevens 1999; Pey et al. 2003). Even though several experimental (Bjorgo et al. 1998; Gamez et al. 2000; Gjetting et al. 2001; Waters et al. 2000) and computational (Gersting et al. 2008; Pey et al. 2007) investigations have shown that PKU is a protein-misfolding disease, very few studies have sought to understand the (un)folding mechanism of PAH. The effect of biopterin and pharmacological/chemical chaperones in rescuing folding of certain PAH mutants has been documented in the literature (Leandro and Gomez 2008; Martinez et al. 2008). However, biophysical and molecular understanding of the unfolding mechanism has been rare (Knappskog and Haavik 1995; Thorolfsson et al. 2002). Its simple architecture and similar fold to hPAH make cPAH an excellent candidate for folding studies. A recent study has reported that iron enhances the kinetic stability of thermophilic PAH at the optimal growth temperature of *Chloroflexus aurantiacus* (Pey and Martinez 2009). Furthermore, preparations of apo- and holo-cPAH, with different divalent metals such as iron, zinc, and cobalt (Zoidakis et al. 2005), are facile allowing investigation of the metal cofactor effect on the folding profile. While the human enzyme can be demetallated (Olafsdottir and Martinez 1999), the chemical denaturation of mammalian PAH is not reversible, which prevents detailed thermodynamic analysis of its folding dynamics.

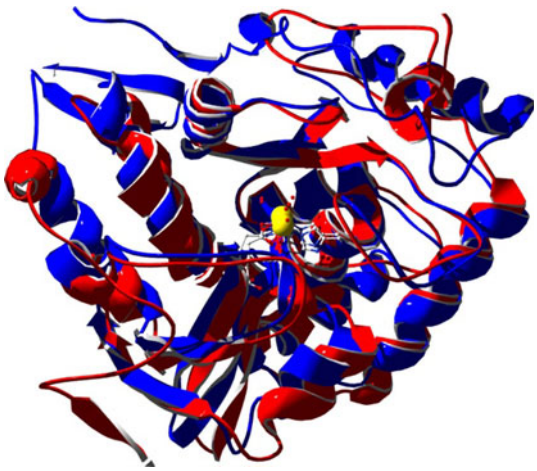

Fig. 1 Catalytic domain of human phenylalanine hydroxylase (hPAH) and bacterial PAH (cPAH) are structurally identical. Superposition of hPAH catalytic domain (*blue*) on cPAH (*red*) yields a 1.2 Å RMSD. Also shown is the active site including iron(III) atom (*yellow sphere*) and 2His1Glu facial triad. Both structures were obtained from PDB (1LTZ, cPAH and 1KWO, hPAH). Structures were analyzed with SWISS-PDB viewer v3.7 and rendered with POVRay v3.6

In this contribution, we present thermodynamic data on the chemical (un)folding of wild-type cPAH and show two distinct folding pathways for apo- and holo-cPAH. Circular dichroism (CD) studies of holo-cPAH with Fe^{II} as well as Co^{II} show a two-state (un)folding transition while apo-cPAH displays an apparent three-state (un)folding transition with a populated intermediate (apo-cPAH^{I}) at 2.2–3.0 M guanidine HCl. Analytical ultracentrifugation (AUC) was employed to characterize distinct equilibrated states in the unfolding pathway for apo- and holo-cPAH

including apo-cPAH^{I}. AUC data show clear metal-mediated differences in the populated species during chemical unfolding. These results underscore the metal's importance in PAH folding as well as the need for tight control against aggregation of PAH.

Methods

Enzyme expression and purification

Chromobacterium violaceum phenylalanine hydroxylase (cPAH) was expressed in *E. coli* BL21 (DE3) pLysS bacterial host according to a previously published procedure (Volner et al. 2003). Recombinant cPAH was purified via chromatography (DEAE-cellulose followed by gel filtration on Sephadex G-75), collected fractions of cPAH were concentrated to 750 μM and stored at −80°C, protein concentration was determined spectrophotometrically, and enzyme activity measurements were performed by following tyrosine production at 275 nm as described previously (Volner et al. 2003).

Spectroscopic analysis of chemical unfolding of apo- and holo-cPAH: UV circular dichroism

Purified cPAH samples were exchanged from LS (50 mM Tris, 50 mM NaCl, pH 7.40) to 5 mM Hepes, pH 7.4 using Ammicon (Millipore) filters with 30,000 MW cut off. Co-cPAH was prepared using apo-cPAH (in 5 mM Hepes pH 7.40) and introducing five equivalents of Co^{II} solution prepared by dissolving $CoCl_2$ (Sigma) in 5 mM Hepes pH 7.40. The fully active form of the enzyme Fe-cPAH was prepared by adding to apo-cPAH (in 5 mM Hepes, pH 7.40) five equivalents of ferrous ammonium sulfate (Sigma) in 5 mM Hepes pH 7.40. Protein samples of concentrations ranging from 6 to 12 μM were incubated and allowed to equilibrate with guanidine HCl concentrations ranging from 0 to 5 M for 3–24 h at 25°C prior to performing the unfolding assay. The range in time of incubation reflects the time for apo- or holo-protein to equilibrate in guanidine HCl. Protein samples incubated in high concentrations of denaturant reached equilibrium faster than those incubated in lower guanidine concentrations. Upon equilibration, a 400 μL aliquot was transferred into a 2.00 mm quartz cuvette (Spectrocell), capped, and analyzed immediately for changes in intrinsic ellipticity at 222 nm using a Jasco J-715 spectropolarimeter. CD spectra were recorded at 0.5 nm increments from 200 to 300 nm using an integration time of 1 s. CD data were normalized to percent of secondary structure per Eq. 1 (Woody 2004). Y corresponds to CD signal at 222 nm (CD_{222}), Y_N is CD_{222} signal for native cPAH^{N}, and Y_U is CD_{222} signal for unfolded protein. The resulting equilibrium unfolding curves were analyzed by two and three state models using Eqs. 2 and 3, respectively (Muralidhar et al. 2005).

$$\%\text{folded} = \frac{Y - Y_U}{Y_N - Y_U} \times 100 \tag{1}$$

$$Y = \frac{Y_N + Y_U \exp - \frac{\Delta G^\circ - m[D]}{RT}}{1 + \exp - \frac{\Delta G^\circ - m[D]}{RT}} \tag{2}$$

$$Y = \frac{Y_N + Y_1 \exp - \frac{\Delta G_1^\circ - m_1[D]}{RT} + Y_U \exp \frac{\left(\Delta G_1^\circ + \Delta G_2^\circ - (m_1 m_2)[D]\right)}{RT}}{1 + \exp - \frac{\Delta G_1^\circ - m_1[D]}{RT} + \exp - \frac{\left(\Delta G_1^\circ + \Delta G_2^\circ - (m_1 m_2)[D]\right)}{RT}} \tag{3}$$

ΔG_1, ΔG_2, and ΔG_3 are changes in Gibbs free energy for three states in equilibrium, Y_U and Y_N are the CD signals for denatured and native protein, respectively, Y_1 is the spectral signal of the intermediate state; m describes the denaturant dependence on Gibbs free energy (kJ mol^{-1} M^{-1}), and its value is a good indicator of the amount of accessible protein surface area resulting from the unfolding reaction (Myers et al. 1995). R is the universal gas constant and T is temperature.

8-Anilino-1-naphthalene sulfonic acid (ANS) fluorescence

ANS (Sigma) was used to probe the hydrophobic regions in cPAH as a function of guanidine concentration. ANS binding studies were done in 5 mM Tris HCl, pH 7.4, at 25.0 ± 0.5°C. ANS, cPAH, and guanidine solutions were prepared in 5 mM Tris HCl, pH 7.40. ANS binding experiments were carried out by incubating 4.8 μM (native or guanidine-denatured) cPAH in 100 μM ANS in 5 mM Tris HCl, pH 7.40 for 2 h. Binding was monitored by ANS fluorescence using an excitation λ of 405 nm, and the emission spectra were recorded from 420 to 600 nm. Fluorescence data was acquired with a FluoroLog®-3 spectrofluorometer (HORIBA Jobin-Yvon).

Electron paramagnetic resonance (EPR) spectroscopy

Spectra were recorded at 4 K on a Bruker ESP 300E EPR spectrometer equipped with an HP 5350B microwave frequency counter, an Oxford ITC4 temperature controller, and a VC40 gas flow controller (for liquid He).

Dynamic light scattering

Biophysical characterization of native and denatured forms of apo- and holo-cPAH was carried out via photon correlation spectroscopy (PCS), also known as dynamic light scattering (DLS). DLS experiments were performed at pH

7.4, 25°C, on a DynaPro99 (Wyatt Technology) equipped with an 832 nm laser and a thermocouple temperature control device. Solvent refractive index was calculated using a refractometer. Solvent density was calculated according to Kawahara and Tanford (1966). All solutions, including buffers, guanidine HCl, native, and denatured protein samples were filtered using 0.22 μm Millex-GV Filter Unit (Millipore). Twenty measurements were recorded per sample, average values are reported for translational diffusion coefficients (D) and Stokes radii (R_h). D is obtained from the autocorrelation function of the scattered light and used to obtain R_h by using the Stokes-Einstein equation (Eq. 4):

$$D = \frac{kT}{f} = \frac{kT}{6\pi\eta R_h} \quad (4)$$

where k is the Boltzmann constant, T is the temperature of the sample, f is the frictional coefficient for a compact sphere in viscous medium, and η is solvent viscosity. Data were analyzed using DYNAMICS^{TM} V5.26.60 software.

Transmission electron microscopy (TEM)

All samples prepared for TEM were negatively stained with uranyl acetate to induce the contrast required for imaging. All solutions, including buffers, guanidine HCl, native, and denatured protein samples were filtered using 0.22 μm Millex-GV Filter Unit (Millipore). The grids were imaged using a Philips CM-100 TEM, operating at 100 kV.

Analytical ultracentrifugation (AUC)

Biophysical characterization of native and denatured apo- and holo-cPAH by analytical ultracentrifugation (AUC) was carried out on a Beckman XL-I Analytical Ultracentrifuge (Beckman-Coulter, Fullerton, CA, USA) at 20°C with 5 mM ammonium acetate, pH 7.40 buffer and varying concentrations of protein and guanidine HCl solutions. The protein concentrations ranged from 0.1 to 1 mg/ml, and all protein solutions (native and denatured) were allowed to equilibrate for at least 4 h prior to each run, which included at least a 1 h temperature equilibrium run at 0 rpm. In particular, we sought to characterize any highly populated species resulting from equilibrium unfolding. The sedimentation velocity experiments were conducted at 50,000 rpm and 20°C, and scans were taken at 3–5 min intervals using both Rayleigh interference optics and absorbance at either 250 or 280 nm. The sedimentation coefficients and apparent molecular weights were calculated from size distribution analyses, both c(s) and ls−g*(s), using SEDFIT (Brown and Schuck 2006; Laue et al. 1992; Schuck 2000). The solvent density, viscosity, and partial specific volume of the protein were calculated using SEDNTERP$^{\&}$ v. 1.09 (http://www.rasmb.bbri.org/rasmb/windows/sednterp-philo).

Results and discussion

Equilibrium unfolding of Apo-cPAH

Apo-cPAH was denatured in guanidine HCl at 25°C in 5 mM Hepes, pH 7.40, and its unfolding reaction was studied at equilibrium by far UV CD, taking advantage of the high chromaticity of the peptide bond, which possesses low energy $n\pi^*$ and higher energy $\pi\pi^*$ amide transitions directed along the carbonyl bond and along the NO direction, respectively (Woody 1996). CD spectra of native apo-cPAH contained negative, broad absorption bands at 212–215 and 222 nm, which are characteristic of alpha helix-containing proteins. Incubation of native apo-cPAH with increasing amounts of guanidine HCl coincided with a decrease in alpha helical absorption bands, which gave way to a single negative band at 215 nm characteristic of random coil structure. Normalization of the CD_{222} signal yielded a distinct unfolding curve, relative to holo-cPAH (see next section), that is characteristic of three states in solution, including a well populated intermediate (apo-cPAH^I) at 2.2–3.0 M guanidine HCl (Fig. 2).

Analysis of the unfolding curve reveals that apo-cPAH is 10-fold less stable than the metallated holo-cPAH. Apo-cPAH^I was found to populate at 2.2–3.0 M guanidine HCl and retains ~30% of its native α-helices. Equilibrium unfolding thermodynamic parameters for apo-cPAH were

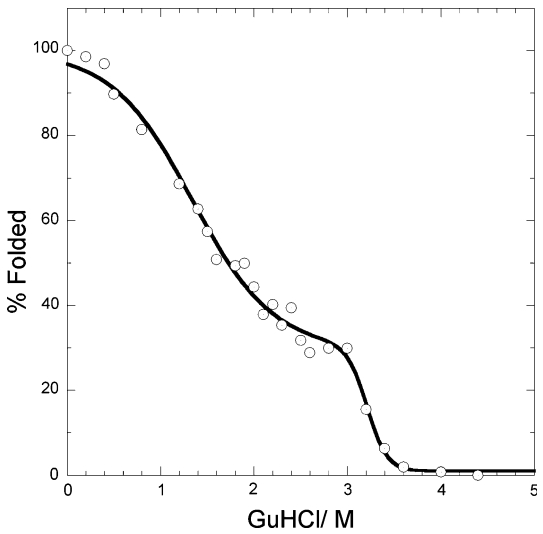

Fig. 2 Three-state unfolding of apo-cPAH. Unfolding transition curve showing the guanidine dependence on apo-cPAH's secondary structure (alpha helical content). Changes in ellipticity at 222 nm were normalized and plotted against guanidine HCl, and fitted to a three state model

obtained via a three-state (un)folding model and are summarized in Table 1. The first phase of unfolding yielded a Gibbs free energy in buffer (ΔG^{N-I}) of 5.2 kJ mol^{-1} and m value (m^{N-I}) of 5.4 kJ mol^{-1} M^{-1}. The second phase of unfolding yielded a Gibbs free energy in buffer (ΔG^{I-U}) of 19.2 kJ mol^{-1} and an m value (m^{I-U}) of 6.3 kJ mol^{-1} M^{-1} for a global Gibbs free energy of unfolding (ΔG^{N-U}) of 24.4 kJ mol^{-1} and m value (m^{N-U}) of 11.7 kJ mol^{-1} M^{-1}. Analysis of apo-cPAH^{I} and the denatured state (apo-cPAH^{U}) in 4 M guanidine HCl with DICHROWEB (Lees et al. 2006) predicted that the former has 24% alpha helical, 26% beta strand, and 50% random coil content, while the latter has 9% alpha helical, 43% beta strand, and 48% random coil content. A word of caution is in order. The exact percentages of the secondary structure analysis of the CD data could be affected by aggregated protein formation and should not be taken as definitive.

The inherent cooperative protein unfolding makes identification and isolation of intermediates challenging. Most folding intermediates are kinetic transients and not populated significantly at equilibrium. In such cases, characterization of an intermediate is achieved by ϕ-value analysis (Fersht and Sato 2004). In this study, however, a well populated intermediate at 2.2–3.0 M guanidine HCl was observed for apo-cPAH. Refolding of apo-cPAH from 5.0 M denatured state (apo-cPAH^{U}) results in a folding curve that traces closely to the unfolding curve [see the Electronic Supplementary Material (ESM)], suggesting that this is an obligatory intermediate on the folding path. The CD spectra of refolded protein also match that of the native form (ESM). Furthermore, incubation of apo-cPAH with guanidine HCl >3 M results in loss of the apo-cPAH^{I} CD_{222} signal suggesting that the intermediate is stabilized by noncovalent interactions.

Equilibrium unfolding of holo-cPAH

Holo-cPAH was denatured with guanidine HCl at 25°C in 5 mM Hepes, pH 7.4. Equilibrated samples were then analyzed by far UV circular dichroism. X-ray diffraction analysis of the native structures of apo- and holo-cPAH showed small differences in RMSD values between apo- and Fe-cPAH (Erlandsen et al. 2002). Consistent with those studies, CD analysis of native apo-, Fe-, and Co-cPAH showed that the proteins are quite similar, possessing negative absorption bands at 212 and 222 nm, which are characteristic of α-helix proteins. Furthermore, optimum hydroxylase activity was restored once iron was added to apo- and Co-cPAH, suggesting that we indeed were starting with proteins in their native state. Equilibrium unfolding studies of Co- and Fe-cPAH analyzed by CD yielded a two-state unfolding curve (Fig. 3). Co- and Fe-cPAH unfolding profiles show that the protein retains ≥90% of its secondary structure in guanidine concentrations of ≤1.5 M. The transition from native to denatured is observed at concentrations ca. higher than 1.8 M, with transition midpoints ($C_{1/2}$) of ~2.8 and 3.3 M guanidine for Fe-cPAH and Co-cPAH, respectively. Refolding of holo-cPAH restores ca. 75% of the CD signal of the native protein (ESM), allowing for detailed quantitative analysis of the thermodynamics of unfolding.

Equilibrium unfolding thermodynamic parameters were obtained via a two-state (un)folding model, resulting in Gibbs free energies of unfolding in the absence of denaturant (ΔG_{H2O}) of 24 and 39 kJ mol^{-1} (Table 1). The difference in chemical (un)folding stability ($\Delta\Delta G$ = 15 kJ mol^{-1}) is consistent with differences in metal binding stability previously obtained by isothermal titration calorimetry (ITC) (Loaiza et al. 2008). The resulting Gibbs free energy underscores the stabilizing effects that iron and

Table 1 Thermodynamic parameters of unfolding for apo- versus holo-cPAH[a]

Enzyme form	ΔG_{H2O} (kJ mol^{-1})	m (kJ mol^{-1} M^{-1})
Apo-cPAH		
ΔG^{N-I}, m^{N-I}	5.2 ± 0.4	5.4 ± 0.4
ΔG^{I-U}, m^{I-U}	19 ± 2	6.3 ± 0.8
ΔG^{N-U}, m^{N-U}	24 ± 2	12 ± 1
Fe-cPAH	24 ± 4	9 ± 1
Co-cPAH	39 ± 4	13 ± 1

[a] Unfolding reactions were followed by CD at 222 nm, 25°C, in 5 mM Hepes, pH 7.40. Parameters and errors were obtained directly from two-state (holo-cPAH) and three-state (apo-cPAH) curve fits

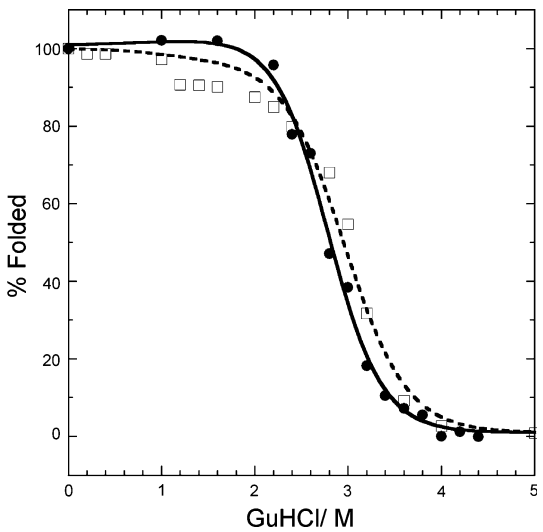

Fig. 3 Two-state unfolding of holo-cPAH. Unfolding transition curves showing the guanidine dependence on Co-cPAH (*squares*) and Fe-cPAH (*circles*) alpha helical content. Changes in ellipticity at 222 nm were normalized and plotted against guanidine HCl, and fitted to a two-state model

cobalt have on the overall protein structure in the presence of chemical denaturant. At first glance, comparison of the total free energy for the unfolding of Fe- and apo-cPAH, which are identical, does not illustrate the stabilizing effect that iron has on the native structure. Nevertheless, analysis of the first stage of apo-cPAH unfolding reveals iron's stabilizing effect. In the absence of iron (or cobalt), native apo-cPAH is quite unstable and requires only a modest 5 kJ mol^{-1} to significantly disrupt its tertiary and secondary structure. The majority of apo-cPAH's stability derives from its intermediate state (apo-$cPAH^{I}$).

The denaturant dependence on the free energy change between two states (*m* value) was also determined. Values of 13 and 9 kJ mol^{-1} M^{-1} were calculated for Co-cPAH and Fe-cPAH, respectively. The higher denaturant dependence on the Gibbs free energy of unfolding observed for Co-cPAH suggests a more cooperative unfolding process and a larger solvent-exposed surface area for Co-cPAH. CD spectra of holo- and apo-cPAH incubated with >4 M guanidine are quite distinct in comparison to those of the native forms. The two peaks at 212 and 222 nm are replaced by a single peak at 215 nm, which is characteristic of a denatured protein that has lost most if not all of its native α-helical content and exists in solution predominantly as a random coil, although the presence of some β-sheet content cannot be ruled out. In fact, analysis of the denatured state of Co-cPAH in 5 M guanidine using DICHROWEB shows this state as having 10% alpha helical content, 45% beta sheet, and 45% random coil.

Unfolding transitions suggest distinct mechanisms for apo- and holo-cPAH and that metal binding appears to protect against intermediate formation. However, it is not evident why cPAH, which evolved to use Fe(II) for catalysis, displays metal promiscuity and higher affinity for divalent metals such as zinc, copper, and cobalt in comparison to eukaryotic PAH. Erlandsen et al. (2002) hypothesized that the observed higher catalytic activity in cPAH can be attributed to solvent-exposed active site and lack of a regulatory domain. The higher affinity for non-native divalent metals in cPAH might be an evolutionary relic that was eventually selected against in eukaryotic forms. An evolutionary compensation arises in which eukaryotic PAH gains metal selectivity and catalytic regulation but sacrifices catalytic turnover frequency.

8-Anilino-1-naphthalene sulfonic acid (ANS) fluorescence

Since Weber and Laurence showed that ANS emission increases by two orders of magnitude in the presence of bovine serum albumin (Laurence 1952; Weber 1952), ANS has been used extensively to probe exposure of protein hydrophobic cores in folding studies (Goto and Fink 1989; Mann and Matthews 1993). ANS fluorescence emission intensity at 380 nm increases sevenfold, relative to no enzyme control, in the presence of apo-cPAH. The emission intensity rises to a maximum at 0.80 M GuHCl and drops off at higher denaturant concentrations. The emission spectra of ANS show a blue shift in the presence of apo-cPAH. In comparison, Fe- and Co-cPAH display an increase in ANS emission intensity at 480 nm with increasing denaturant concentrations to maxima at [GuHCl] = 1.8 and 2.2 M, respectively. Holo-cPAH also results in a blue shift of the ANS emission spectrum. The relative concentrations of GuHCl needed to reach maximum emission intensity increased along the series apo- < Fe- < Co-cPAH. The increase in ANS emission intensity in the presence of cPAH at increasing [GuHCl] indicates exposure of the hydrophobic core and binding of ANS. Thus, hydrophobic core exposure for apo-cPAH occurs at lower denaturant concentrations than those observed for Fe- and Co-cPAH. Thus, metal binding in the active site enhances the stability of the tertiary structure minimizing exposure of the protein's hydrophobic core. This finding is consistent with the observation from the CD studies, which probed disruption of α-helical contacts, i.e., secondary structure.

Dynamic light scattering (DLS) and transmission electron microscopy (TEM)

Characterization of native and denatured states of apo-cPAH using dynamic light scattering shows a guanidine-dependent increase in radii between native and denatured forms of apo-cPAH. Hydrodynamic radii (R_H) of native apo-$cPAH^{N}$, apo-$cPAH^{I}$ (at 2.6 M GuHCl), and denatured apo-$cPAH^{U}$ (at 5.0 M GuHCl) are 3.5, 41, and 13.2 nm, respectively. The R_H value of 41 nm for apo-$cPAH^{I}$ is an order of magnitude larger than native apo-$cPAH^{N}$. Intermediates that are well populated tend to fall into two basic categories; they are either native-like or not. Among the native-like is the molten globule state, which is often referred to as an extended native form because it resembles the native secondary structure but lacks the tertiary characteristics of the native state, leading to a less compact conformation. Our DLS results, along with the CD and AUC data (discussed next), show that apo-$cPAH^{I}$ is not a molten globule. Instead, the biophysical data favor an oligomeric species, most likely an aggregate, as the more probable structure of apo-$cPAH^{I}$. This claim is corroborated by TEM micrographs of apo-$cPAH^{I}$ (apo-cPAH in 2.6 M GuHCl), which show varying sizes of protein aggregates with some >40 nm in diameter.

Analytical ultracentrifugation (AUC)

It is understood that proteins in solution are not restricted to a single conformation, instead they sample different energetically equivalent conformations. Similarly, when a protein's structure is perturbed its conformation equilibrium will be too. Spectroscopic methods such as CD and UV-vis report an average of conformers in solution. AUC has the advantage of detecting different populations of conformers in solution as long as their structural differences affect their sedimentation properties. Equilibrium unfolding of apo-, Fe-, and Co-cPAH was analyzed by AUC. Sedimentation velocity analysis shows a clear difference between apo-cPAH and holo-cPAH in relation to the species that populate under denaturing conditions. Sedimentation velocity analysis of both apo-cPAH and holo-cPAH, in the absence of guandinium hydrochloride, show a predominant species responsible for ~90% of the total signal with a sedimentation coefficient (s20,w) of 2.9 S (R_H = 3–4 nm and apparent MW = 34–35 kDa), which correlates to a momoner of the protein. CD analysis of the unfolding of apo-cPAH shows a highly populated intermediate (apo-cPAH^I) in the range of 2.2–3.0 M guanidine HCl. When apo-cPAH^I in 2.4 M GuHCl is subjected to sedimentation velocity analysis, the ls−g*(s) of the sample yields multiple species in solution undetected by other spectroscopic methods employed in this study. Whereas only 10% of the total species detected sediments at s20,w = 2.6 S, which is assigned to residual native-like apo-cPAH^N (Fig. 4), most of the material, 90% of the signal, had a weight average s20,w of about 48 S. Relative to holo-cPAH, the AUC signal for the native apo-cPAH^I is broader with a significantly higher s20,w and with a higher s shoulder resulting from an overlapping species with similar sedimentation properties. This intermediate is also seen at guanidine concentrations of 3.0 M, but lost at [GuHCl] ≥ 4.0 M (Fig. 4). Disappearance of the intermediate species at 4.0 M guanidine coincides with the emergence of two species. The major is characterized by a sharp peak centered at s20,w = 2.6 S, accounting for 64% of the signal. Another sharp peak characterizes the minor species that contributes 24% of the signal with s20,w = 1.8 S. The broad signal observed for apo-cPAH^I complicates the fitting and does not permit reliable determinations of radii and molecular weight. Nevertheless, it can be estimated that the intermediate states (referred to herein collectively as apo-cPAH^I) represent an aggregate comprised of at least 40 monomeric enzyme units.

Analytical ultracentrifugation analyses were conducted on holo-cPAH with the native metal cofactor Fe(II) and its inorganic surrogate Co(II). Fe-cPAH in the absence of guanidine HCl shows a major species that accounts for 88% of the total signal and has s20,w, R_H, and apparent MW values of 2.9 S, 2.6 nm, and 33,300 Da, respectively. These values are comparable to apo-cPAH^N (see above). AUC of Fe-cPAH in 5.0 M GuHCl showed one major species (86% of the signal) with sedimentation coefficient s20,w = 1.8 S (corrected for solvent viscosity, etc.) and R_H = 4.7 nm (Fig. 5). By comparison, under the same conditions (≥4.0 M GuHCl), the apo-cPAH showed two distinct species at 1.8 and 2.6 S. This difference indicates a possible equilibrium process induced by the metal cofactor on the timescale of the centrifugation. Another plausible explanation is that the metal influences formation of these species suggesting a different transition state during unfolding. The bottom line is the sedimentation coefficient shows that the unfolded species Fe-cPAH^U is monomeric and more expanded than apo-cPAH. At an intermediate denaturant concentration of 2.8 M GuHCl, Fe-cPAH partitions into two species. A broad peak in the ls−g*(s) plot (Fig. 5) was detected with an s20,w ≈ 25 S alongside a native-like species at s20,w = 2.3 S. The species at 25 S seems to be distinct species that went undetected by spectroscopic means (CD analysis). A similar minor species is also observed for Co-cPAH at intermediate GuHCl (see below).

The active state of the enzyme is Fe(II), which is air-sensitive. All manipulations and sample preparations were carried out in an inert-atmosphere box. Nevertheless, we needed to confirm that samples subjected to AUC were not oxidized to Fe(III). Before and after AUC runs, the Fe-cPAH was examined by EPR spectroscopy. Non-heme Fe(II) does not have an EPR feature under normal perpendicular mode at 4 K, while Fe(III) displays a distinct signal in the g = 4 region depending on rhombicity. EPR spectra collected before and after the AUC experiments with holo-cPAH showed no EPR signal, indicating that the obtained results are indeed for Fe(II).

AUC analysis of Co-cPAH followed the same pattern observed for Fe-cPAH. In 1.0 M guanidine HCl, Co-cPAH shows a major species that accounts for 96% of the total signal, has s20,w, R_H, and apparent MW values of 2.9 S, 2.9 nm, and 35,500 Da, respectively (Fig. 6). These values are comparable to those observed for native Fe-cPAH^N (see above). Increasing the concentration of GuHCl to 2.3 M gave rise to a minor species at s20,w ≈ 18.8 S (Fig. 6). The major species, 2.6 S, is comparable to the native form of the enzyme. AUC of Co-cPAH in >5.0 M GuHCl showed one major species (92% of the signal) with sedimentation coefficient s20,w = 1.8 S (corrected for solvent viscosity, etc.), and R_H = 4.8 nm. This signal is again identical to the unfolded protein with Fe(II), Fe-cPAH^U, showing that the unfolded species Co-cPAH^U is monomeric and more expanded than apo-cPAH^U.

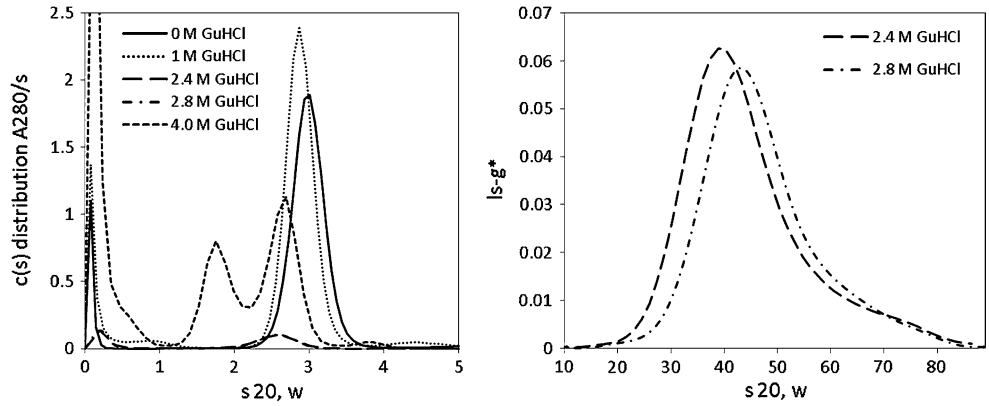

Fig. 4 AUC of apo-cPAH and characterization of the aggregate intermediates. Sedimentation velocity study for the unfolding of apo-cPAH in the presence of varying concentrations of guanidinium ion. The plots of c(s) and ls−g*(s) distributions were evaluated using SedFit. The plots are scaled to a constant total concentration of 1 absorbance unit where the total concentration is the sum of the slow and fast components. The identities of the lines are indicated in the figure, and sedimentation coefficients are corrected to 20°C and water

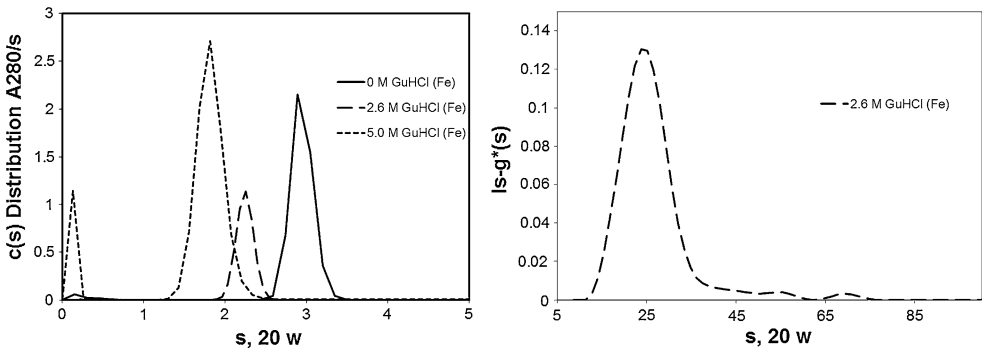

Fig. 5 AUC of native and denatured Fe-cPAH. Sedimentation velocity study for the unfolding of Fe-cPAH in the presence of varying concentrations of denaturant (GuHCl). Size distribution analysis [c(s) and ls−g*(s)] of the Fe-cPAH was evaluated using Sedfit. At 2.8 M GuHCl, in addition to native Fe-cPAH^{N}, another species is detected at 25 S. At 5.0 M GuHCl a single species at s20,w = 1.8 S is observed

Fig. 6 AUC of native and denatured Co-cPAH. The influence of Co(II) on the unfolding of cPAH. At 2.8 M and 3.3 GuHCl, in addition to native Co-cPAH^{N}, several minor species were detected in the range of 10–30 S. At 5.0 M GuHCl, one species was observed (corrected s20,w of 1.8 S)

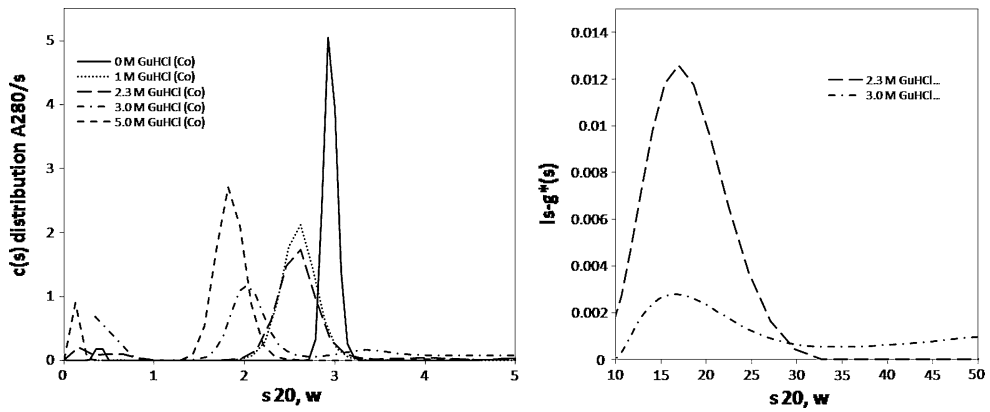

Conclusion

We have investigated the equilibrium (un)folding of apo- and holo-cPAH using guanidine HCl. Our equilibrium folding studies shed light on (1) the folding mechanism at the catalytic domain and (2) the effects the metal cofactor plays on said mechanism. CD analysis shows two-state unfolding transition curves for Fe- and Co-cPAH and three-state unfolding curve for apo-cPAH with a populated intermediate over the range of 2.2–3.0 M guanidine.

Thermodynamic analyses give a ΔG_{H2O} for Co-cPAH of 39 kJ mol^{-1}, ΔG_{H2O} for Fe-cPAH of 24 kJ mol^{-1}, and a global ΔG_{H2O} of 24 kJ mol^{-1} for apo-cPAH. The majority of the stability for the latter comes from the intermediate unfolded state(s) of apo-cPAH^{I} (19 kJ mol^{-1}). Comparison of *m* values suggests a more extended final denatured state for holo-cPAH. Analysis of apo-cPAH^{I} by DLS yields $R_H = 40$ nm, and AUC data corroborate an aggregate species at s20,w = 41 S, not seen in holo-cPAH. Altogether, our data are most consistent with a two-state (un)folding mechanism for holo-cPAH, and multi-state with populated aggregate intermediate(s) for apo-cPAH.

The differences in folding curves between apo- and holo-cPAH reveal differences in their respective folding mechanisms. Several studies depicting the importance of metals in protein (un)folding have appeared in the literature recently (Hussain and Wittung-Stafshede 2007; Michel and Bren 2008; Sedlak et al. 2008). Herein, we have shown that while this is true for cPAH, the metal also protects from accumulation of an aggregate intermediate state(s) (apo-cPAH^{I}) during protein folding. Stability studies on wild-type hPAH denatured with urea in the presence versus absence of L-Phe show a multi-state unfolding mechanism as well as a substrate-dependent aggregation at urea concentrations <2 M (Kleppe et al. 1999). The observed stability and protection against aggregation in our study may have important ramifications on the relationship between metal delivery and proper folding, and the implication of the latter in PKU.

Acknowledgments We wish to thank the U.S. National Science Foundation for financial support of this work through grants CHE-0502391 and CHE-0749572.

References

Abu-Omar MM, Loaiza A, Hontzeas N (2005) Reaction mechanisms of mononuclear non-heme iron oxygenases. Chem Rev 105:2227–2252

Bjorgo E, Knappskog PM, Martinez A, Stevens RC, Flatmark T (1998) Partial characterization of three-dimensional structural localization of eight mutations in exon 7 of the human phenylalanine hydroxylase gene associated with phenylketonuria. Eur J Biochem 257:1–10

Brown PH, Schuck P (2006) Macromolecular size and shape distributions by sedimentation velocity analytical ultracentrifugation. Biophys J 90:4651–4661

Carr RT, Balasubramanian S, Hawkins PCD, Benkovic SJ (1995) Mechanism of metal-independent hydroxylation by *Chromobacterium violaceum* phenylalanine hydroxylase. Biochemistry 34:7525–7532

Chen D, Frey P (1998) Phenylalanine hydroxylase from *Chromobacterium violaceum*. Uncoupled oxidation of tetrahydropterin and the role of iron in hydroxylation. J Biol Chem 273:25594–25601

Erlandsen H, Stevens RC (1999) The structural basis of phenylketonuria. Mol Genet Metab 68:103–125

Erlandsen H, Kim JY, Patch MG, Han A, Volner A, Abu-Omar MM, Stevens RC (2002) Structural comparison of bacterial and human iron-dependent phenylalanine hydroxylases: similar fold, different stability and reaction rates. J Mol Biol 320:645–661

Fersht AR, Sato S (2004) ϕ-Value analysis and the nature of protein-folding transition states. Proc Natl Acad Sci USA 101:7976–7981

Fitzpatrick PF (2003) Mechanism of aromatic amino acid hydroxylation. Biochemistry 42:14083–14091

Fusetti F, Erlandsen H, Flatmark T, Stevens RC (1998) Structure of tetrameric human phenylalanine hydroxylase and its implications for phenylketonuria. J Biol Chem 273:16962–16967

Gamez A, Perez B, Ugarte M, Desviat LR (2000) Expression analysis of phenylketonuria mutations: effect on folding and stability of the phenylalanine hydroxylase protein. J Biol Chem 275: 29737–29742

Gersting SW, Kemter KF, Staudigl M, Messing DD, Danecka MK, Lagler FB, Sommerhoff CP, Roscher AA, Muntau AC (2008) Loss of function in phenylketonuria is caused by impaired molecular motions and conformational instability. Am J Hum Genet 83:5–17

Gjetting T, Petersen M, Guldberg P, Guttler F (2001) In vitro expression of 34 naturally occurring mutant variants of phenylalanine hydroxylase: correlation with metabolic phenotypes and susceptibility toward protein aggregation. Mol Genet Metab 72:132–143

Goto Y, Fink AL (1989) Conformational state in beta-lactamase: molten-globule states at acidic and alkaline pH with high salt. Biochemistry 28:945–952

Hussain F, Wittung-Stafshede P (2007) Copper binding increases thermodynamic stability of bacterial (CopZ) and human (Atox1) copper chaperones. Biochim Biophys Acta 1774:1316–1322

Kappock TJ, Caradonna JP (1996) Pterin-dependent amino acid hydroxylases. Chem Rev 96:2659–2756

Kawahara K, Tanford C (1966) Viscosity and density of aqueous solutions of urea and guanidine hydrochloride. J Biol Chem 241:3228–3232

Kleppe R, Uhlemann K, Knappskog PM, Haavik J (1999) Urea-induced denaturation of human phenylalanine hydroxylase. J Biol Chem 274:33251–33258

Knappskog PM, Haavik J (1995) Tryptophan fluorescence of human phenylalanine hydroxylase produced in *Escherichia coli*. Biochemistry 34:11790–11799

Kobe B, Jennings IG, House CM, Michell BJ, Goodwill KE, Santarsiero BD, Stevens RC, Cotton RG, Kemp BE (1999) Structural basis of autoregulation of phenylalanine hydroxylase. Nat Struct Biol 6:442–448

Laue TM, Shah BD, Ridgeway TM, Pelletier SL (1992) Computer-aided interpretation of analytical sedimentation data for proteins. In: Harding SE et al (eds) Analytical ultracentrifugation in biochemistry and polymer science. The Royal Society of Chemistry, Cambridge, pp 90–125

Laurence DJ (1952) A study of the adsorption of dyes on bovine serum albumin by the method of polarization of fluorescence. Biochem J 51:168–180

Leandro P, Gomez CM (2008) Protein misfolding in conformational disorders: rescue of folding defects and chemical chaperoning. Mini Rev Med Chem 8:901–911

Lees JG, Miles AJ, Wien F, Wallace BA (2006) A reference database for circular dichroism spectroscopy covering fold and secondary structure space. Bioinformatics 22:1955–1962

Loaiza A, Armstrong KM, Baker BM, Abu-Omar MM (2008) Kinetics of thermal unfolding of phenylalanine hydroxylase containing different metal cofactors (Fe^{II}, Co^{II}, and Zn^{II}) and their isokinetic relationship. Inorg Chem 47:4877–4883

Mann CJ, Matthews CR (1993) Structure and stability of an early folding intermediate of *Escherichia coli* trp aporepressor

measured by far-UV stopped-flow circular dichroism and 8-anilino-1-naphthalene sulfonate binding. Biochemistry 32:5282–5290

Martinez A, Calvo AC, Teigen K, Pey AL (2008) Rescuing proteins of low kinetic stability by chaperones and natural ligands: phenylketonuria, a case study. Mol Biol Prot Folding 83:89

Michel LV, Bren KL (2008) Submolecular unfolding units of *Pseudomonas aeruginosa* cytochrome c551. J Biol Inorg Chem 13:837–845

Muralidhar D, Jobby MK, Krishnan K, Annapurna V, Chary KV, Jeromin A, Sharma Y (2005) Equilibrium unfolding of neuronal calcium sensor-1. N-terminal myristoylation influences unfolding and reduces protein stiffening in the presence of calcium. J Biol Chem 280:15569–15578

Myers JK, Pace CN, Scholtz JM (1995) Denaturant m values and heat capacity changes: relation to changes in accessible surface areas of protein unfolding. Protein Sci 4:2138–2148

Olafsdottir S, Martinez A (1999) The accessibility of iron at the active site of recombinant human phenylalanine hydroxylase to water as studied by ^{1}H NMR paramagnetic relaxation. J Biol Chem 274:6280–6284

Panay AJ, Fitzpatrick PF (2008) Kinetic isotope effects on aromatic and benzylic hydroxylation by *Chromobacterium violaceum* phenylalanine hydroxylase as probes of chemical mechanism and reactivity. Biochemistry 47:11118–11124

Pember SO, Villafranca JJ, Benkovic SJ (1986) Phenylalanine hydroxylase from *Chromobacterium violaceum* is a copper-containing monooxygenase. Kinetics of the reductive activation of the enzyme. Biochemistry 25:611–6619

Pey AL, Martinez A (2009) Iron binding effects on the kinetic stability and unfolding energetics of a thermophilic phenylalanine hydroxylase from *Chloroflexus aurantiacus*. J Biol Inorg Chem 14:521–531

Pey AL, Desviat LR, Gamez A, Ugarte M, Perez B (2003) Phenylketonuria: genotype–phenotype correlations based on expression analysis of structural and functional mutations in PAH. Hum Mutat 21:370–378

Pey AL, Stricher F, Serrano L, Martinez A (2007) Predicted effects of missense mutations on native-state stability account for phenotypic outcome in phenylketonuria, a paradigm of misfolding diseases. Am J Hum Genet 81:1006–1024

Schuck P (2000) Size distribution analysis of macromolecules by sedimentation velocity ultracentrifugation and Lamm equation modelling. Biophys J 78:1606–1619

Sedlak E, Ziegler L, Kosman DJ, Wittung-Stafshede P (2008) In vitro unfolding of yeast multicopper oxidase Fet3p variants reveals unique role of each metal site. Proc Natl Acad Sci USA 105:19258–19263

Thorolfsson M, Ibarra-Molero B, Fojan P, Petersen SB, Sanchez-Ruiz JM, Martinez A (2002) L-phenylalanine binding and domain organization in human phenylalanine hydroxylase: a differential scanning calorimetry study. Biochemistry 41:7573–7585

Volner A, Zoidakis J, Abu-Omar MM (2003) Order of substrate binding in bacterial phenylalanine hydroxylase and its mechanistic implication for pterin-dependent oxygenases. J Biol Inorg Chem 8:121–128

Waters PJ, Parniak MA, Akerman BR, Scriver CR (2000) Characterization of phenylketonuria missense substitutions, distant from the phenylalanine hydroxylase active site, illustrates a paradigm for mechanism and potential modulation of phenotype. Mol Genet Metab 69:101–110

Weber G (1952) Polarization of the fluorescence of macromolecules. 2. Fluorescence conjugates of ovalbumin and bovine serum albumin. Biochem J 51:155–167

Woody RW (1996) Theory of circular dichroism of proteins. In: Fasman GD (ed) Circular dichroism and the conformational analysis of biomolecules. Plenum, New York, pp 25–67

Woody RW (2004) Circular dichroism of protein folding intermediates. Methods Enzymol 380:242–285

Zoidakis J, Loaiza A, Vu K, Abu-Omar MM (2005) Effect of temperature, pH, and metals on the stability and activity of phenylalanine hydroxylase from *Chromobacterium violaceum*. J Inorg Biochem 99:771–775